Reduction of modal noise due to fiber/photodetector misalignment in SSMF links based on 850 nm VCSELs through a low-cost polymer coupling structure

Published Version:
Reduction of modal noise due to fiber/photodetector misalignment in SSMF links based on 850 nm VCSELs through a low-cost polymer coupling structure / Nanni J.; Viana C.; Tegegne Z.G.; Tartarini G.; Algani C.; Polleux J.-L.. - In: APPLIED OPTICS. - ISSN 1559-128X. - ELETTRONICO. - 59:8(2020), pp. 2329-2336. [10.1364/AO.380976]

Availability:
This version is available at: https://hdl.handle.net/11585/752067 since: 2023-03-15

Published:
DOI: http://doi.org/10.1364/AO.380976

Jacopo Nanni, Carlos Viana, Zerihun Gedeb Tegegne, Giovanni Tartarini, Catherine Algani, and Jean-Luc Polleux,

Reduction of modal noise due to fiber/photodetector misalignment in SSMF links based on 850 nm VCSELs through a low-cost polymer coupling structure

In: Applied Optics 59, 2329-2336 (2020)

The final published version is available online at:

https://doi.org/10.1364/AO.380976

Reduction of Modal Noise due to Fiber / Photodetector Misalignment in SSMF Links based on 850nm VCSELs through a Low-Cost Polymer Coupling Structure

JACOPO NANNI[1,*], CARLOS VIANA[2], ZERIHUN GEDEB TEGEGNE[3], GIOVANNI TARTARINI[1], CATHERINE ALGANI[4], AND JEAN-LUC POLLEUX[2,3,4]

[1] *Department of Electrical, Electronic and Information Engineering, University of Bologna, 40136, Bologna, Italy*
[2] *ICON Photonics, 77420, Champs-sur-Marne, France*
[3] *ESIEE Paris, ESYCOM, Université Paris-Est, 93160, Noisy-le-Grand, France*
[4] *ESYCOM, Le Cnam, Paris, 75003, France*
[*] *Corresponding author: jacopo.nanni3@unibo.it*

Compiled January 9, 2020

A low cost polymer-based structure is proposed to improve the coupling between fiber end section and photodetector active surface in optical links based on Standard Single Mode Fiber (SSMF) which employ Vertical Cavity Surface Emitting Lasers (VCSELs) operating at 850nm, i.e below the SSMF cut-off wavelength. Considering as receivers small area detectors, which are generally necessary to guarantee high-speed operation, but at the same time are particularly subject to power fluctuations due to modal noise (whose impact is in turn enhanced in presence of fiber-to-photodetector misalignment), significant achievements are demonstrated by employing the presented structure. Indeed, in presence of a misalignment of ±4 to ±6 μm, which is nowadays typically achievable, the relative optical power fluctuations due to modal noise reduce in the presented case more than 4 times (2.5% from more than 10%) with respect to the case of butt-coupling, which implies an increase of the same factor in the output Signal to Noise Ratio at the receiver end.

OCIS codes: (060.2330) Fiber optics communications; (250.5460) Polymer waveguides

http://dx.doi.org/10.1364/ao.XX.XXXXXX

1. INTRODUCTION

Optical infrastructures based on Standard Single Mode Fibers (SSMFs) are widespread deployed, mainly because, at wavelengths λ greater than the cutoff value $\lambda_c \simeq 1260nm$, their single mode operation entails a great exploitability for present and future high speed applications. Indeed, using the Multimode fiber (MMF) or, for short connections, the Plastic Optical Fiber (POF), the bandwidth-length product would sooner or later stop to satisfy the ever growing bandwidth request of the final user, leading to a frequent need of infrastructure upgrading.

Visiting typical vendors websites, it can be seen that, as an additional attractive feature, the SSMF has reached nowadays a lower price-over-meter if compared to the MMF, for connections equal or greater than a few hundred meters length, thanks to its simple manufacturing process and widespread diffusion in the market. This aspect, in conjunction with the fact that in many instances a capillary SSMF network is already available, makes the use of this infrastructure attractive for all those applications in which a major objective to be reached is to keep at low levels the global cost of the whole optical system.

Examples in this context include optical systems operating at $\lambda < \lambda_c$, like those based on short-λ Vertical Cavity Surface Emitting Lasers (VCSELs), which indeed exhibit as attractive features a low fabrication cost and a low energy consumption together with a high modulation bandwidth. In addition, the combination of their typical values of adiabatic chirp coefficient and optical power emitted make them, for short to medium range connections, to be a cheap and efficient alternative to Distributed Feedback Lasers (DFBs) operating at 1310 or 1550 nm, in which the high values of adiabatic frequency chirp can be source of impairments [1–4], while the high value of power emitted can determine undesired noise produced by back-scattering effects [5–7].

Actually, at present these devices are not typically used with SSMFs, since, due to their limited core area and step-index profile, the resulting optical system risks to feature relatively high degrees of laser-to-fiber coupling losses and intermodal dispersion. MMFs or POFs can constitute in this view a preferable option because their larger core area and/or their graded-index profile guarantee in principle lower coupling losses and higher transmission bandwidths [8–10].

However important investigations have been recently undertaken with the aim to move the use of such devices to optical systems where a single mode or quasi-single mode operation is obtained. In particular, the use of 1060 nm VCSELs realized in GaAs technology, has been reported in the context of datacenter networks, where the error-free baseband data-transmission of 50 Gbit/s has been recently achieved utilizing 1km of a non-standard fiber exhibiting single mode behavior at that λ [11]. Moreover, in the context of the wireless coverage of in- and outdoor environments, 850 nm VCSEL-based systems have been demonstrated which confirm the possibility to exploit SSMF-based optical connections [12–15].

With reference to this last scenario, in order to exploit the mentioned attractive features of VCSELs for high speed signal transmission, SSMFs must be coupled to high-speed photodetectors which are generally characterized by small detecting areas. If the technique employed to couple optical fibers and photodetectors consists in the so called "butt-coupling", this fact risks to cause high levels of relative fluctuations of the received photocurrent due to the phenomenon of modal noise.

Indeed, in presence of a small detecting area, utilizing this simple solution, which consists in directly attaching the fiber to the device [16], even short values of the misalignment between the center of the active surface of the photodetector and the center of the fiber end section (fiber-to-photodetector misalignment, FPM) can cause non-negligible values of the overlap integral between the two different Linearly Polarized (LP) modes propagating within the SSMF for $\lambda = 850nm$ [17, 18]. This fact determines even at short distances the mentioned presence of photocurrent fluctuations, which, excluding cases of beneficial exploitability for particular characterization measurements [19], are in general undesired since they typically lead to the presence of distortion terms and/or to the decrease of the Signal to Noise Ratio (SNR) both in Analog and Digital Optical Connections [20–22].

Solutions which reduce the impact of modal noise have then been proposed in literature, for example applying a preventive-mode filtering operation, useful also to remove intermodal dispersion [23–25], or superimposing a low frequency modulation tone [26] in order to have a less coherent source and therefore mitigate modes interference effects.

However, if the effects of FPM are reduced through an appropriate coupling device, the modal noise issue can, in principle, be preventively solved, without the need of additional external components, filters or signals. In this view, possible solutions are those based on micro optical elements such as lenses/ ball-lenses, which, however, must be placed and actively aligned to the device, adding overall extra costs and complexity at the packaging stage [27–29]. Within the same view, a solution for realizing a fiber / photodetector coupling structure which maintains low cost features, can be obtained through the so called ICON technology [30], which is based on an integrated polymer-based waveguide realized through a collective monolithic wafer level process. This technology showed, with reference to SSMF-based links operating at 1550 nm, to maintain at high levels the value of the received optical power even in presence of important FPMs [31].

In the present work, it will be shown that applying the ICON technology to 850nm SSMF-based optical links, a great reduction of the impact of modal noise can be obtained. This result, which is a connected to the capability of this technology to mitigate the effects of FPMs, leads to an important increase of the global system performance.

The paper is organized as follows. In Section 2 the mathematical model describing the modal noise in the considered optical link will be illustrated. In particular, the quantities to be appropriately controlled in view of maintaining its effects at low levels will be evidenced. Section 3 describes the design and realization of the taper structure illustrating the theoretical results in terms of coupling and tolerance to FPMs obtained with a simulation tool based on the Beam Propagation Method (BPM). In Section 4 the evaluation of the beneficial effect in terms of reduced impact of modal noise are described, in agreement with the model proposed in Section 2. Finally Conclusions will be drawn in Section 5.

2. MODAL NOISE IMPACT: MATHEMATICAL MODEL

The impairments produced by modal noise in optical link performances have been studied with reference to MMFs [32, 33], POFs [34] and SSMFs operating below the nominal cut-off wavelength [25]. The last scenario is particularly critical for $\lambda = 850\,nm$, because in this case the presence of practically just two propagating modes enhances the effect of modal noise.

To model mathematically this operating condition, a single wavelength source is considered, emitting at the optical frequency ω_{opt} and producing the transmission electrical field $E_{opt}(t)$, which, at the input section of the SSMF, reads as:

$$\vec{E}_{opt}(t) = E_0 e^{j\omega_{opt} t}\vec{e} \tag{1}$$

where $E_0 = \sqrt{P_0}$, P_0 is the optical power emitted and $\vec{e}$ represents the normalized electrical field.

Considering the presence of two SSMFs connected (as the case of a simple pigtail connected to a span of fiber) of length z_1 and z_2, respectively, the power carried by two modes of amplitudes A_1 and A_2 at the end section of the second fiber can be written as follows [33]:

$$\begin{aligned}&\vec{E}_{opt}(t, z_1 + z_2) = \\ &\vec{E}_0 e^{j\omega_{opt} t} \sum_{m=1}^{2}\sum_{n=1}^{2} A_m A_n a_{nm} \vec{e}_m^{(2)} e^{-j\left[\beta_n^{(1)}(t) z_1 + \beta_m^{(2)}(t) z_2\right]}\end{aligned} \tag{2}$$

In (2) $\beta_k^i(t)$ (i,k=1,2) is the propagation constant of the k–th mode of the i–th fiber, which is assumed to exhibit a variation in time because of changes in environmental quantities, like temperature. Furthermore, $\vec{e}_m^{(2)}$ is the normalized field of the m–th mode of the second fiber, and A_1, A_2 are considered so that $\sum_i A_i^2 = 1$. Finally, the value a_{nm} represents the mode matching coefficient between the n–th mode of the first fiber and the m–th mode of the second fiber defined as follows:

$$a_{nm} = \int_{S_\infty} \vec{e}_n^{(1)} \cdot \vec{e}_m^{*(2)}\, dS, \quad n, m = 1, 2 \tag{3}$$

The square of a_{nm} represents then, the power coupled between the n–th mode of the first fiber with the m–th mode of the second fiber, which indeed is determined by the connector misalignment.

Not considering, for the sake of clarity, the contributions of sources of noise different from modal noise (e.g. shot, RIN), the optical power received at the detector can be written as

$$P(t) = \int_{S_{PD}} |\vec{E}_{opt}(t, z_1 + z_2)|^2 dS = \mu_{opt} + \Delta P_{opt}(t) \quad \textbf{(4)}$$

where S_{PD} is the surface area of the photodetector, while the mean value (μ_{opt}) and the fluctuation (ΔP_{opt}) of the received optical power can be straightforwardly derived as follows:

$$\mu_{opt} = P_0 \sum_{m=1}^{2} \sum_{n=1}^{2} A_n^2 a_{nm}^2 b_{mm} \quad \textbf{(5)}$$

$$\Delta P_{opt}(t) =$$
$$2P_0 \sum_{m=1}^{2} A_1 A_2 a_{1m} a_{2m} b_{mm} \cos\left[\Delta\beta_{12}^{(1)}(t) z_1\right] +$$
$$2P_0 \sum_{n=1}^{2} \sum_{k=1}^{2} A_n A_k a_{n1} a_{k2} b_{12} \cos\left[\Delta\beta_{nk}^{(1)}(t) z_1 + \Delta\beta_{12}^{(2)}(t) z_2\right] \quad \textbf{(6)}$$

In Eq. (5) and Eq. (6) $\Delta\beta_{nk}^{(i)} = \beta_n^{(i)}(t) - \beta_k^{(i)}(t)$ and the b_{nm} terms are defined in the following way:

$$b_{nm} = \int_{S_{PD}} \vec{e}_n^{\,(2)} \cdot \vec{e}_m^{\,*(2)}\, dS, \quad n, m = 1, 2 \quad \textbf{(7)}$$

Due to the orthonormality property of the normalized modes' fields, if S_{PD} were infinitely extended, it would be $b_{mm} = 1$. However, due to the finite value of the area S_{PD}, it is typically $b_{mm} < 1$, and the value of b_{mm} represents then the corresponding power loss of the m–th mode. Analogously, the term b_{12} would be equal to zero if S_{PD} were infinitely extended. This would imply absence of fluctuations of the received power (see Eq. (6)), regardless of the presence of FPM. However, due to the finite value of the area S_{PD}, in presence of FPM the collecting surface "seen" by the modes loses some degree of symmetry. This determines a non-orthonormality of the modes' fields, which results in an increase of b_{12} with respect to the value (theoretically $b_{12} = 0$) that it exhibits in absence of FPM, and consequently causes fluctuations of the received power.

The expression of the standard deviation of the received power σ_{opt} can then be computed as:

$$\sigma_{opt} = \sqrt{var(\Delta P_{opt})} \quad \textbf{(8)}$$

It is now possible to determine the expression of the relative fluctuation of the optical received power Γ_{opt}, which is typically utilized to quantify the impact of modal noise in optical links [35], and is given by:

$$\Gamma_{opt} = \frac{\sigma_{opt}}{\mu_{opt}} \quad \textbf{(9)}$$

The model just illustrated shows that to keep modal noise under control, it is necessary that Γ_{opt} keeps low values under the typical operating conditions. Failure to fulfill this requirement would determine serious problems, in particular for reduced area photodetector. Indeed, in this case, even small FPMs can easily result in a reduction of μ_{opt}, due to the decrease of the effective photodetector receiving area, and, at the same time, in a possible increase of σ_{opt} due to the variation of the quantity b_{12} mentioned above. This fact is clearly shown in Figure 1, in which the quantities μ_{opt}, σ_{opt} (both normalized to P_0) and Γ_{opt}

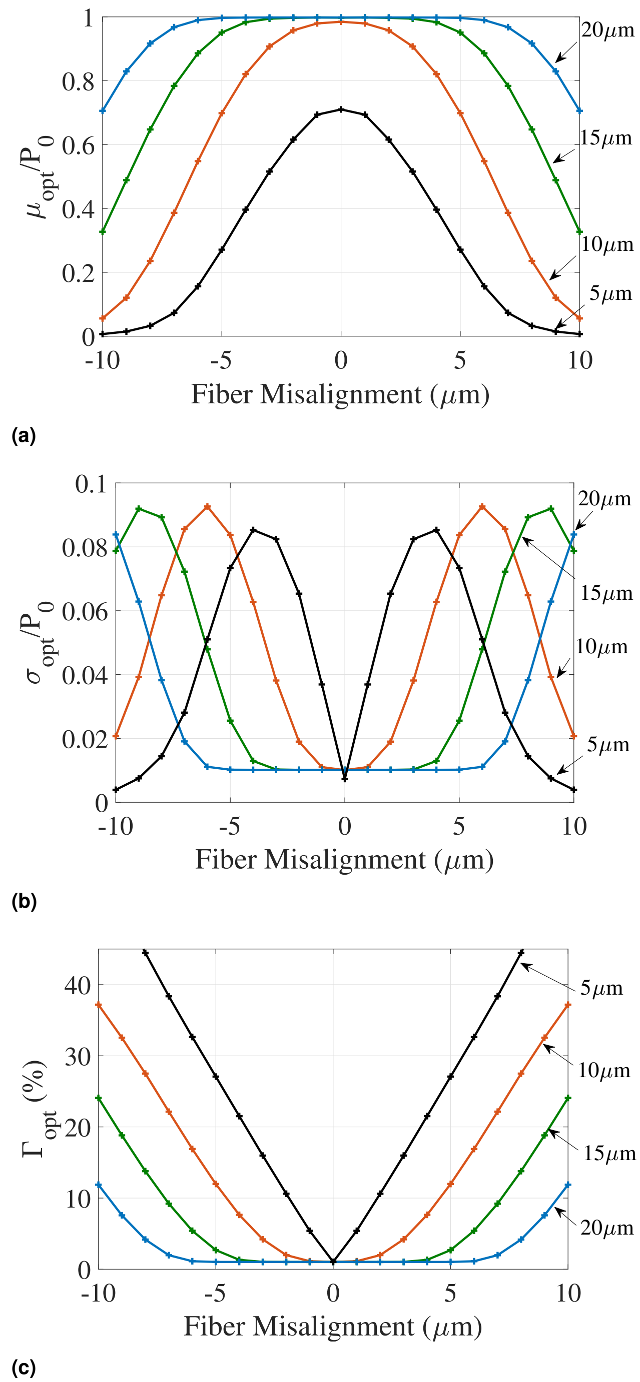

Fig. 1. Example of modeled values of μ_{opt}/P_0 (a), σ_{opt}/P_0 (b) and Γ_{opt} (c) as a function of the value of FPM, for different values of the photodetector diameter. See text for details.

(expressed in percentage) are separately modeled as functions of the value of FPM for different detector active areas. The model considers the case in which the two modes have the same power, i.e. $A_1^2 = A_2^2 = 0.5$, and the misalignment between the two fibers is 0.25μm.

As mentioned in the Introduction, aim of the work here presented is precisely to demonstrate that utilizing the polymeric taper realized through the ICON technology to improve the coupling between fiber end section and photodetector active area, the twofold result of maintaining μ_{opt} at high values and maintaining σ_{opt} at low values can be obtained in front of a wide range of values for the FPM, globally resulting in a low value of Γ_{opt}. As opposed to that, in front of the same range of values of FPM the butt-coupling would in general determine high values of Γ_{opt} due to the variation of the quantity b_{12} mentioned above.

3. DESIGN AND REALIZATION OF THE PROPOSED STRUCTURE

A. Structure description

The fabricated 3D coupling structure is realized with a vertical tapered waveguide made of SU-8 polymer, to be placed in direct contact with the active device as shown in Figs. 2a and 2b.

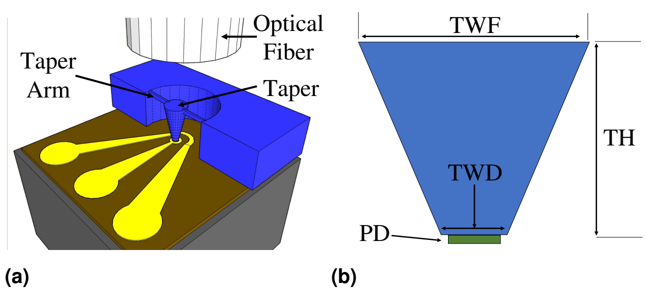

Fig. 2. 3D (a) and side (b) view of the polymer-based structure and its parameters. In particular, TWF: Taper width in contact with the fiber, TWD: Taper width in contact with the photodiode and TH: Height of the taper.

The physical realization of the structure is based on the process described in [30]. This process starts with the spin-coating of SU-8 on the desired wafer of devices, followed by a controlled dose of UV light exposure given in absence of wavelength filters, controlling properly in this way the angle of the taper. Moreover, to increase the robustness and mechanical stability of the structure, an anchoring system (taper arm) is designed allowing it to maintain its vertical position without altering the propagation (see Fig. 2a). This last operation exploits the privileged partial isotropy of the photolithographic process under exposure of the resist material. The whole structure is then manufactured in the same volume of SU-8 by exploiting a single photolithography step.

In this way, differently from other techniques which require an active alignment (as for example the placement of mechanical receptacle ball lenses), an intermediate optical coupling structure is present, giving high optical coupling efficiency η and large tolerance to misalignment. A direct consequence is that both optical alignment and assembly process become passive, since it is not required to bias the active device during the alignment, so that the use of high precision and expensive equipment is not necessary.

Note that η is defined as the ratio of the quantities μ_{opt} and

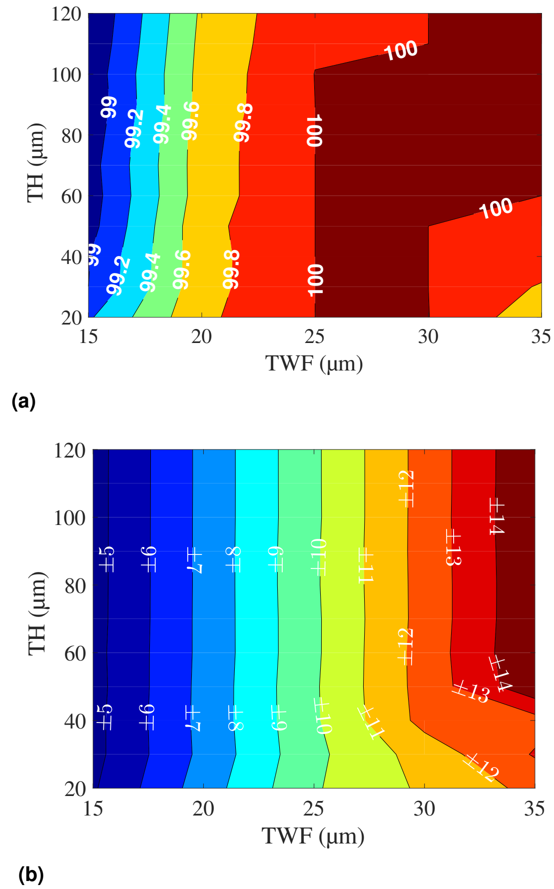

Fig. 3. Simulation results of the proposed taper structure at 850nm a) Coupling efficiency η as function of TWF and TH, b) 1dB alignment tolerance as a function of TWF and TH.

P_0 defined in Section 2. It therefore gives an immediate information on the behavior of the average received power μ_{opt}, since it represents the normalized version of such quantity.

B. Design Parameters determination

Through numerical simulations, which have been performed assuming the structure to be coupled with a photodetector with an active area of 10 μm, it has been possible to evidence a great improvement, with respect to the butt-coupling case, of the 1dB tolerance to misalignment of the coupling efficiency, defined as the misalignment value at which the coupling efficiency decreases by 1dB with respect to its maximum value.

The analysis has been performed with the use of the BeamPROP tool from RSOFT© software based on BPM. The simulation has been performed considering a fiber diameter of 9μm, a core refractive index of 1.468, a numerical aperture of 0.13 and taking into account the propagation of both the fundamental LP_{01} and the high order LP_{11} modes with the same level of amplitude.

Figures 3a and 3b show the behavior of the received power efficiency and the 1dB tolerance misalignment, respectively, as function of the height of the taper TH and of the top side cone diameter TWF, by fixing the value of TWD = 11μm and the PD active area side at 10 μm.

Fig. 3a suggests that for TWF higher than 23-24μm, the power efficiency could be increased up to 100%, and that even for smaller values of TWF it would not however go below 99%. This can ben explained by the fact that at 850nm the field shape is highly concentrated into the fiber core [36] if compared to higher wavelengths. Moreover, Fig. 3b shows that for TH>50μm the 1dB alignment tolerance increases almost proportionally for increasing TWF independently on TH.

According to Figure 3 the height has a limited impact in the range of study, as the opening angle of the cone is limited. Therefore combining these simulation results with the technological process considerations, the structure employed has been designed to have TH=100μm, TWD=11μm and TWF=25μm in order to provide the best mechanical stability and robustness to the structure together with satisfying 1dB tolerance performances.

4. PERFORMANCE EVALUATION OF THE PROPOSED STRUCTURE

A. Setup utilized

The experimental setup utilized is depicted in Figure 4.

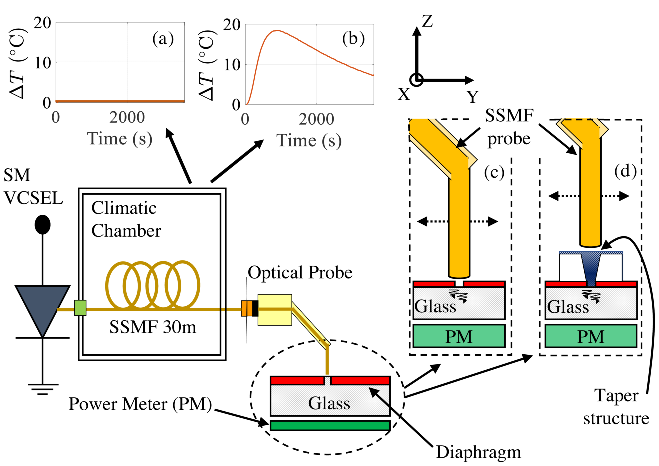

Fig. 4. Experimental setup based on diaphragm approach. The two arrows starting from the climatic chamber indicate the two temperature regimes utilized for evaluating respectively the received power in the XY plane in stable environmental conditions(a) and the relative power fluctuations caused by modal noise in front of temperature variations (b). The two arrows starting from the diaphragm indicate its detailed structure when testing respectively butt-coupling (c) and ICON technology (d). See text for further details.

An 850nm single mode (SM) VCSEL was coupled to a short pigtail of SSMF, followed by 30 meters of G.652 fiber placed inside a climatic chamber, whose purpose was twofold. At first, the temperature was kept constant (see the correspondent behavior of ΔT versus time in Figure 4), in order to evaluate in a stable environment the behavior of the received optical power in presence of various FPMs within the plane (XY). This measurement aimed to evaluate μ_{opt} in the considered FPM range, comparing the cases of utilization of the ICON technology and butt coupling. Subsequently, FPM was let to vary within a chosen direction in the XY plane considered, and controlled temperature variations were forced with $\pm$ 1°C/min maximum slope in the fiber (see again the correspondent behavior of ΔT versus time). This second measurement aimed to evaluate the power fluctuations due to modal noise, comparing in the cases of utilization of the ICON technology and butt coupling the quantities σ_{opt} and Γ_{opt}. To perform the measurements, the output of the climatic chamber was connected to an optical probe which was set perpendicularly to the wafer under test. The probe was further movable by using a nano-positioner in order to control the misalignment between the fiber and the structure considered (see again Figure 4).

To have at disposal an optical receiver with known collecting characteristics, an Aluminum-based diaphragm which emulates the active area of a photodiode was placed over a glass substrate, below which an optical power meter was placed, based on a detector with wide active area. The metallic diaphragm was used to define with certainty the size of the photodetector (10 μm diameter in the present case) and measure, even without the use of a physical device, the amount of light which impacts the surface by creating an equivalent configuration. In particular, when the butt coupling configuration was tested, (see Figure 4 (a)) the fiber end section was directly illuminating the diaphragm. Instead, when the ICON polymeric taper was tested, (see Figure 4 (b)) the fiber end section was illuminating its larger section (width TWF), while its shorter section (width TWD) was directly connected to the diaphragm.

All the structures were directly fabricated in cleanroom, guaranteeing a direct availability. As the process is simple, they could be realized very easily and with high repeatability, including adhesion of SU-8 on glass, which proved to be excellent.

B. Average received power

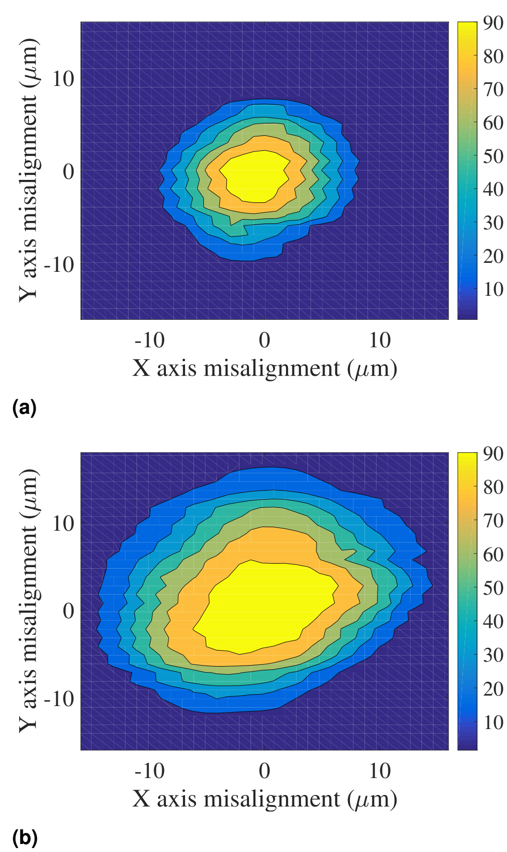

Fig. 5. XY plane view of the coupling efficiency in case of butt-coupling (a) and ICON technology (b).

Figures 5a and 5b give a complete view of the measured values at constant temperature of $\eta = \mu_{opt}/P_0$, for varying values of the fiber misalignment in the XY plane, where the value of P_0 was measured as the optical power received by the power meter in absence of glass, diaphragm and ICON polymeric taper. The higher value of μ_{opt}/P_0 obtainable with the ICON technology with respect to the butt coupling is confirmed for all the values of FPM in the XY plane.

It can be however observed that, while figure 5a presents a substantially symmetric behavior, an asymmetry is observable in Figure 5b, which can be related to the real physical shape of the structure realized with the ICON technology. Due to the presence of this asymmetry, the value of 1dB tolerance improvement depends on the angle of slice. However, the 1dB tolerance is always greater than $\pm 7.5\ \mu$m, reaching a maximum value of $\pm 9\ \mu$m, in front to a value that is always around $\pm 4\ \mu$m in the case of butt-coupling. In addition, the ratio between the two areas for which the efficiency loss is lower than 1dB results to be about $175\mu m^2/50\mu m^2 = 3.5$ indicating an important average improvement of μ_{opt}/P_0 exhibited by ICON technology compared to the butt-coupling technique.

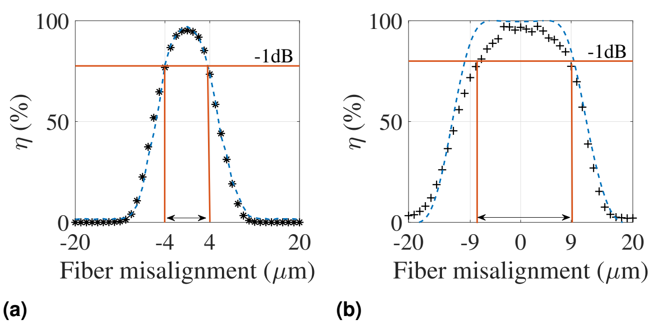

Fig. 6. Slice section measurements (cross and stars) of the power efficiency and corresponding BPM simulations (dashed lines) obtained for the butt-coupling (a) and ICON technology (b) cases. The 1dB fiber misalignment tolerance is also highlighted in the two figures.

Figures 6a and 6b compare experimental and theoretical values of η as a function of FPM in case of butt-coupling and ICON technology coupling, respectively, again at constant temperature. The angle of slice chosen in the ICON technology case was the one giving the largest 1 dB tolerance. The experimental values come from the same measurements which led to figures 5a and 5b, while the theoretical ones result from BPM simulations. A very good agreement between modelled and measured values can be appreciated. The fact that the theoretical 100% of optical coupling efficiency is not exactly reached in the ICON technology case can also in this case be ascribed to the real physical realization of the considered specimen.

C. Fluctuations of the received power

To test the effect of the structure developed on the power fluctuations due to modal noise, the optical probe is progressively placed in several misaligned positions (see again the setup shown in Fig. 4), which ranged from -10 μm to 10 μm taking as reference the results obtained in Figures 6a and 6b. As mentioned previously, in correspondence to each position, the fiber has been exposed to controlled temperature variations of $\pm\ 1°$C/min maximum slope which caused the onset of modal

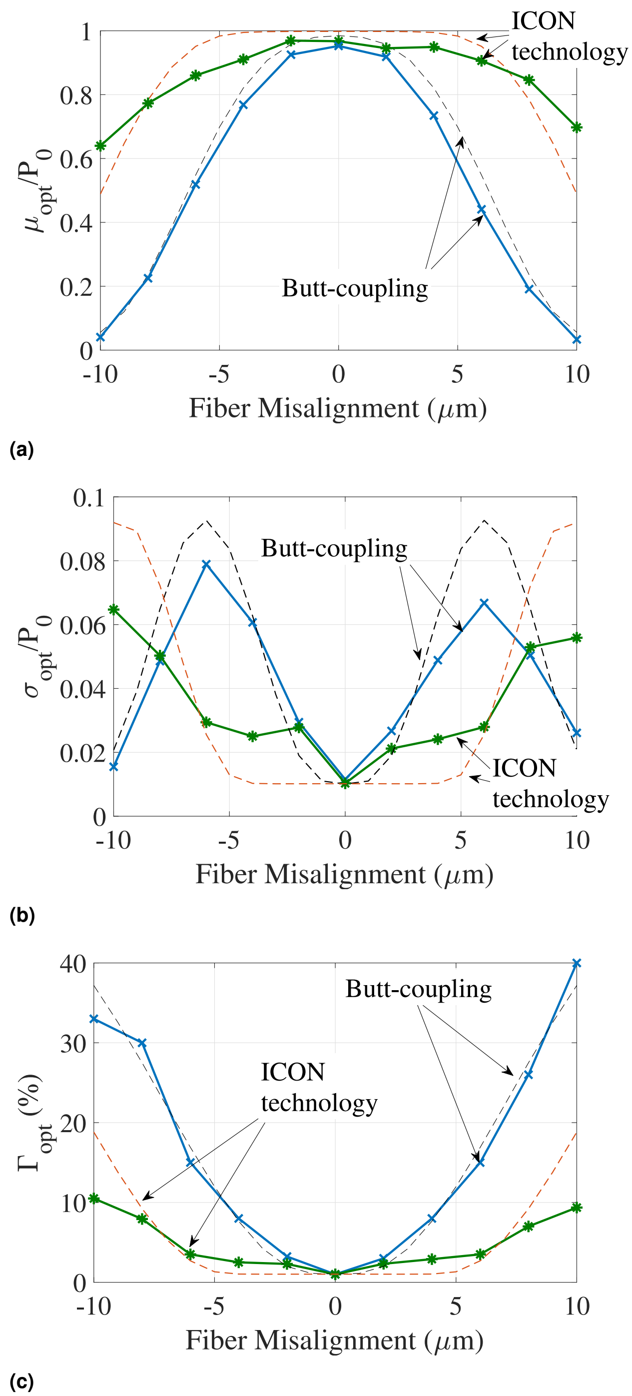

Fig. 7. Measurements (solid lines) and simulations (dashed lines) of μ_{opt}/P_0 (a), σ_{opt}/P_0 (b) and Γ_{opt} (c) in case of 10 μm diameter photodetector for fiber butt-coupling and with ICON technology for which an equivalent aperture size of 17 μm has been estimated.

noise. For each position of the fiber with respect to the photodetector the received optical power has then been measured for a time period of one hour with a sampling time of one second. Both rise and fall temperature slopes were tested in order to increase the reliability of the statistical validation (see inset in Figure 4).

The impact of the fluctuations has then been evaluated through the quantities σ_{opt} Γ_{opt} described in the previous subsection. To apply the developed simulation model in the case of the system exploiting the ICON technology, the 3D taper structure has been approximated with an equivalent 2D photodiode area seen by the fiber, considering for its diameter an appropriate value. With the model developed, this value has been estimated to be 17 μm, in front of 25 μm and 11 μm of top and bottom diameter sizes, respectively. Figure 7 shows the behavior of μ_{opt}, σ_{opt} (normalized to P_0) and Γ_{opt} measured as function of fiber misalignment. It can be appreciated that a significant improvement in the tolerance to optical power fluctuations caused by modal noise is reached when ICON technology is used. For example, in case of fiber misalignment of ± 4 to ± 6 μm, Γ_{opt} passes from 10% in case of butt-coupling to only 2.5% with ICON technology. Being Γ_{opt} proportional to the fluctuations of the link gain expressed in dB [25, 33], which are directly related to the fluctuation of the SNR, a decrease of Γ_{opt} of 4 times leads to a decrease of the SNR fluctuations at least of the same quantity, eventually improving the quality of the transmission. For typical VCSELs parameters the fluctuations of SNR can pass then from some dBs to less than 1 dB, leading to a considerable improvement of performances in both analogue and digital optical systems.

Figure 7c shows that the model of Γ_{opt} fits well the measurements both in butt-coupling case, confirming a diameter of 10 μm for S_{PD}, and in the ICON case, where, as mentioned, an equivalent photodetector diameter of 17 μm has been considered. The validity of the model is also confirmed by the values of μ_{opt} and σ_{opt} shown in Figures 7a and 7b, where the measured values obtained in case of butt-coupling are comparable to the simulation of the case of $10\mu m$ photodetector diameter.

Slight differences between modeled and measured values, referred to the ICON technology, can be appreciated in Figure 7. This can be reasonably ascribed to the approximation taken, in which the 3D coupling structure has been replaced an equivalent 2D collecting surface.

5. CONCLUSION

A polymer-based structure performing the optical coupling between fiber end section and photodiode in optical systems based on Standard Single Mode Fiber operating at 850nm has been presented. The structure proposed, which exploits a passive coupling without requiring expensive active alignment processes, reduces in these systems the impact of modal noise.

In particular, the relative optical power variation coefficient Γ_{opt} passes from 10% for butt-coupling to 2.5% with ICON technology in case of a fiber misalignment of ± 4 to ± 6 μm, reducing the fluctuations of the Signal to Noise Ratio by a factor 4.

Through the mathematical model proposed, it is possible to assume that when utilizing the ICON coupling technology, the receiver utilized, which exhibits a collective area diameter of 10 μm, featured a tolerance to misalignment as if it exhibited a collective area diameter of 17 μm.

In front of this value of equivalent diameter, the properties of the photodetector are not changed, and its performances are consequently maintained, including the capability to detect signals with high electrical bandwidth which is related to the low actual dimensions of its collecting surface.

ACKNOWLEDGMENTS

This work was funded by SATT IdF-Innov as a maturation project and was partly supported by FUI-ORIGIN and FUI-MORF projects.

DISCLOSURE

The authors declare no conflicts of interest.

REFERENCES

1. A. Villafranca, J. Lasobras, and I. Garces, "Precise characterization of the frequency chirp in directly modulated DFB lasers," in *Proceedings of Spanish Conference on Electronic Devices,* (Madrid, Spain, 2007), pp. 173–176.
2. J. Nanni, M. Barbiroli, F. Fuschini, D. Masotti, J.-L. Polleux, C. Algani, and G. Tartarini, "Chirp evaluation of semiconductor DFB lasers through a simple Interferometry-Based (IB) technique," Appl. Opt. **55**, 7788–7795 (2016).
3. G. Meslener, "Chromatic dispersion induced distortion of modulated monochromatic light employing direct detection," IEEE J. Quantum Electron. **20**, 1208–1216 (1984).
4. M. U. Hadi, J. Nanni, J.-L. Polleux, P. A. Traverso, and G. Tartarini, "Direct digital predistortion technique for the compensation of laser chirp and fiber dispersion in long haul radio over fiber links," Opt. Quantum Electron. **51**, 205 (2019).
5. P. Gysel and R. K. Staubli, "Spectral properties of Rayleigh backscattered light from single-mode fibers caused by a modulated probe signal," J. Light. Technol. **8**, 1792–1798 (1990).
6. J. Nanni, A. Giovannini, S. Rusticelli, F. Perini, J. Monari, E. Lenzi, and G. Tartarini, "Challenges due to Rayleigh backscattering in radio over fibre links for the square kilometre array radio-telescope," in *21st International Conference on Transparent Optical Networks (ICTON),* (Angers, France, 2019), pp. 1–4.
7. J. Nanni, A. Giovannini, M. Hadi, S. Rusticelli, F. Perini, J. Monari, E. Lenzi, and G. Tartarini, "Optimum Mitigation of distortion induced by Rayleigh Backscattering in Radio-over-Fiber links for the Square Kilometer Array Radio-Telescope," in *International Topical Meeting on Microwave Photonics (MWP),* (Ottawa, Canada, 2019), pp. 1–4.
8. C. Viana, Z. G. Tegegne, M. Rosales, J. L. Polleux, C. Algani, V. Lecocq, C. Lyszyk, and S. Denet, "Hybrid photo-receiver based on SiGe heterojunction photo-transistor for low-cost 60 GHz intermediate-frequency radio-over-fibre applications," Electron. Lett. **51**, 640–642 (2015).
9. N. N. Ledentsov, V. A. Shchukin, V. P. Kalosha, N. N. Ledentsov, J. Kropp, G. Schaefer, L. Chorchos, and J. P. Turkiewicz, "Development of 850 nm and 910 nm Vertical-Cavity Surface-Emitting Lasers for 50-100 Gb/s Applications," in *21st International Conference on Transparent Optical Networks (ICTON),* (Angers, France, 2019), pp. 1–5.
10. Y. Shi, D. Visani, C. M. Okonkwo, H. Yang, H. P. A. van den Boom, G. Tartarini, E. Tangdiongga, and A. M. J. Koonen, "First demonstration of hd video distribution over large-core pof employing uwb for in-home networks," in *Optical Fiber Communication Conference and Exposition and the National Fiber Optic Engineers Conference,* (2011), pp. 1–3.
11. E. Simpanen, J. S. Gustavsson, A. Larsson, M. Karlsson, W. V. Sorin, S. Mathai, M. R. Tan, and S. R. Bickham, "1060 nm Single-Mode VCSEL and Single-Mode Fiber Links for Long-Reach Optical Interconnects," J. Light. Technol. **37**, 2963–2969 (2019).
12. M. Kowalczyk, G. Stepniak, L. Maksymiuk, and J. Siuzdak, "Transmission in single mode telecom fiber below the cut-off wavelength," Wiley Microw. Opt. Technol. Lett. **59**, 2033–2038 (2017).
13. P. M. Sevila, V. Almenar, and J. L. Corral, "Transmission Over SSMF at 850 nm: Bimodal Propagation and Equalization," IEEE/OSA J. Light. Technol. **35**, 4125–4136 (2017).

14. J. Nanni, J. Polleux, C. Algani, S. Rusticelli, F. Perini, and G. Tartarini, "VCSEL-Based Radio-Over-G652 Fiber System for Short-/Medium-Range MFH Solutions," J. Light. Technol. **36**, 4430–4437 (2018).
15. J. Nanni, L. Fernández, M. U. Hadi, C. Viana, Z. G. Tegegne, J. Polleux, and G. Tartarini, "Multi-channel LTE-over-Fiber system based on 850nm VCSEL and SSMF for low cost, low consumption Front-Hauls," in *21st International Conference on Transparent Optical Networks (ICTON),* (Angers, France, 2019), pp. 1–4.
16. T. Tekin, "Review of Packaging of Optoelectronic, Photonic, and MEMS Components," IEEE J. Sel. Top. Quantum Electron. **17**, 704–719 (2011).
17. J. Nanni, Z. G. Tegegne, C. Viana, G. Tartarini, C. Algani, and J. Polleux, "SiGe Photo-Transistor for Low-Cost SSMF-Based Radio-Over-Fiber Applications at 850nm," IEEE J. Quantum Electron. **55**, 1–9 (2019).
18. J. Nanni, Z. G. Tegegne, C. Algani, G. Tartarini, and J. Polleux, "Use of SiGe Photo-Transistor in RoF links based on VCSEL and standard single mode fiber for low cost LTE applications," in *International Topical Meeting on Microwave Photonics (MWP),* (Touluse, France, 2018), pp. 1–4.
19. J. Nanni, J. Polleux, C. Algani, S. Rusticelli, F. Perini, and G. Tartarini, "Chirp evaluation of 850-nm single mode vcsel exploiting modal noise in standard single mode fiber," IEEE J. Quantum Electron. **54**, 1–11 (2018).
20. R. Epworth, "Modal noise-Causes and cures," Laser Focus. **17**, 109–115 (1981).
21. G. Alcaro, D. Visani, L. Tarlazzi, P. Faccin, and G. Tartarini, "Distortion mechanisms originating from modal noise in radio over multimode fiber links," IEEE Transactions on Microw. Theory Tech. **60**, 185–194 (2012).
22. J. Nanni, G. Tartarini, S. Rusticelli, F. Perini, C. Viana, J. Polleux, and C. Algani, "Modal noise in 850nm VCSEL-based radio over fiber systems for manifold applications," in *Fotonica AEIT Italian Conf. Photonics Technologies,* (Turin, Italy, 2015), pp. 1–4.
23. D. Vez, S. G. Hunziker, R. Kohler, P. Royo, M. Moser, and W. Bachtold, "850 nm vertical-cavity laser pigtailed to standard singlemode fibre for radio over fibre transmission," Electron. Lett. **40**, 1210–1211 (2004).
24. Z. Tian, C. Chen, and D. V. Plant, "850-nm VCSEL Transmission Over Standard Single-Mode Fiber Using Fiber Mode Filter," IEEE Photonics Technol. Lett. **24**, 368–370 (2012).
25. J. Nanni, S. Rusticelli, C. Viana, J. L. Polleux, C. Algani, F. Perini, and G. Tartarini, "Modal Noise Mitigation in 850-nm VCSEL-Based Transmission Systems Over Single-Mode Fiber," IEEE Trans. Microw. Theory Techn. **64**, 3342–3350 (2016).
26. T. Niiho, K. Masuda, H. Sasai, and M. Fuse, "Proposal of RoF transmission system using 850 nm VCSEL and 1.3μm SMF with low-frequency superposition technique," in *Proceedings of Optical Fiber Communication Conference (OFC),* (2006), pp. 1–3.
27. I.-S. Chung, P. Debernardi, Y. T. Lee, and J. Mørk, "Transverse-mode-selectable microlens vertical-cavity surface-emitting laser," Opt. Express **18**, 4138–4147 (2010).
28. T. C. Donald J. Hayes, "Next-generation optoelectronic components enabled by direct-write microprinting technology," in *Proc. SPIE 5435, Enabling Photonic Technologies for Aerospace Applications VI,* (2004).
29. B. Ciftcioglu, R. Berman, J. Zhang, Z. Darling, S. Wang, J. Hu, J. Xue, A. Garg, M. Jain, I. Savidis, D. Moore, M. Huang, E. G. Friedman, G. Wicks, and H. Wu, "A 3-D Integrated Intrachip Free-Space Optical Interconnect for Many-Core Chips," IEEE Photonics Technol. Lett. **23**, 164–166 (2011).
30. J.-L. Polleux and C. Viana, "Structure de couplage optique collective passive de composants optiques et opto-électroniques," (2015). U.S. Patent 118 131 A1.
31. C. Viana, Z. G. Tegegne, J. Nanni, G. Tartarini, C. Algani, F. Marty, N. Pavy, and J. Polleux, "Vertical Optical Coupling Structure Based on Polymer for Small Size and High-Speed Photodetectors," IEEE Photonics Technol. Lett. **30**, 1886–1889 (2018).
32. I. Gasulla and J. Capmany, "Modal noise impact in Radio over Fiber multimode fiber links," Opt. Express **16**, 121–126 (2008).
33. D. Visani, G. Tartarini, M. N. Petersen, L. Tarlazzi, and P. Faccin, "Link Design Rules for Cost-Effective Short-Range Radio Over Multimode Fiber Systems," IEEE Trans. Microw. Theory Tech. **58**, 3144–3153 (2010).
34. M. Matsuura, R. Furukawa, Y. Matsumoto, A. Inoue, and Y. Koike, "Evaluation of modal noise in graded-index silica and plastic optical fiber links for radio over multimode fiber systems," Opt. Express **22**, 6562–6568 (2014).
35. R. Dandliker, A. Bertholds, and F. Maystre, "How modal noise in multimode fibers depends on source spectrum and fiber dispersion," J. Light. Technol. **3**, 7–12 (1985).
36. D. Marcuse, "Loss analysis of single-mode fiber splices," The Bell Syst. Tech. J. **56**, 703–718 (1977).